Trabajo de fin de máster

MÁSTER EN FÍSICA DE LA ATMÓSFERA Y CLIMA

Universidad de Valladolid

Facultad de Ciencias

EFECTO DE LAS NUBES Y LOS AEROSOLES SOBRE LA RADIACIÓN SOLAR ULTRAVIOLETA ESPECTRAL

Autor: Diego Ruiz Ramos

Tutores: Roberto Román Diez
David Mateos Villán

16 de septiembre de 2022

Effect of clouds and aerosols on spectral solar UV radiation

Diego Ruiz Ramos

Supervisors: Roberto Román Diez, David Mateos Villán

Universidad de Valladolid

Abstract

Ultraviolet (UV) radiation is the most energetic among all extraterrestrial sources that reach the Earth, being able to cause multiple effects on live beings inhabiting it. There are numerous factors controlling the amount of radiation reaching, as well as the way it hits the Earth's surface. In this study, the effect of two of the main UV radiation modulators, clouds and aerosols, which can absorb or scatter radiation; is analyzed.

There are simulated data for clear sky conditions at our disposal, obtained by *LibRadtran* radiative transference model. They are validated, in the first place, proving that they are an accurate approximation to experimental data measured on cloud-free sky days. Once their usefulness is certified, cloud and aerosol enhancing or attenuating effect over spectral UV radiation is quantified in the solar UV wavelength range. For this purpose, a cloud characteristic parameter, CMF (*Cloud Modification Factor)*, is calculated as a function of sky cloudiness and solar zenith angle (SZA), while a similar procedure is followed with an aerosol parameter, AMF (*Aerosol Modification Factor)*, calculated as a function of aerosol optical depth (AOD) and SZA.

1. Introduction

The Sun is a star that behaves like a black body whose surface is at an average temperature of 5790 K (de la Casinière and Cachorro, 2008) [1]. It is composed mainly of hydrogen and emits a radiation spectrum according to Planck's law. Being the nearest celestial body to Earth, it is the main source of all the extraterrestrial energy that reaches our atmosphere.

This radiation can be divided into three intervals according to its wavelength, λ, which, from highest to lowest λ are: the near infrared (IR), the *visible* (so called because it contains the wavelengths that are perceptible by the human eye, $\sim$ 400 - 720 nm), and the ultraviolet (UV).

Ultraviolet radiation is electromagnetic radiation with a wavelength of the order of 100 to 400nm, so called because it has wavelengths shorter than the last color in the visible spectrum, violet. Even though it only represents around 5% of terrestrial solar radiation (Diffey, 2002) [2], this type of radiation is the most energetic that reaches our planet, being capable of inducing different effects on the living beings, including, of course, human beings.

Exposure to UV radiation is beneficial in small amounts, e.g., playing a fundamental role in the production and synthesis of vitamin D, necessary for the absorption of calcium and its deposition in the bones (Reichrath and Reichrath, 2012) [3]. In addition, it has been found to be useful to treat various diseases, such as rickets, psoriasis and eczema (WHO, 2003) [4].

However, the effects of said radiation are accumulative, so that a prolonged exposure can cause rapid aging of the skin, as well as different skin and eye diseases: from the well-known sunburns, called erythema, to the various types of skin cancers

(Diffey, 1991) [5], including cataracts or actinic keratitis (WHO, 2003). Furthermore, relationship with a decrease in the effectiveness of the immune system has been verified (Krutmann, 1994) [6].

This radiation arrives at Earth as a part of all the solar radiation that reaches our planet. Therefore, there are several factors on which said arrival and its power, known as irradiance, depend. This is due to the fact that, as it passes through the atmosphere, solar radiation, and therefore UV, undergoes a series of processes basically based on two mechanisms: absorption and dispersion or *scattering*.

Some of the atmospheric factors that cause these phenomena are the gases in the atmosphere, cloudy conditions in the sky or the amount of aerosols suspended in the air. The former interact with solar radiation through *molecular scattering*, also known as Rayleigh scattering (Román, 2014) [7], and through selective absorption, with special attention to ozone O_3 and the layer that this gas forms in the stratosphere. In the case of clouds and aerosols, they do this through what is known as Mie *scattering* and an absorption that varies smoothly with wavelength in the solar range.

Other factors that modulate the radiation levels at the surface are the position of both the Sun and the Earth, the position of the observer with respect to the Sun according to the solar zenith angle (SZA, see section 1.1), the surface albedo or the altitude (Mateos, 2012) [8]. However, these are left out of the study carried out here, which will focus on the analysis of the effect of clouds.

1.1. Solar radiation. Absorption and Rayleigh and Mie scattering

Direct (or *beam*) solar radiation reaches us in a certain direction, marked by the solar zenith angle (SZA), which corresponds to the angle formed by the line joining the observer and the Sun, and the vertical direction; thus being the complementary angle of the solar height. When this radiation passes through the atmosphere, interacting with its components, it is modified by numerous phenomena, leading it to be partially or totally absorbed, as well as scattered with different orientation according to what is known as Rayleigh or Mie scattering, depending on the height of the scatterer particle. Both phenomena cause the extinction of the radiative beam.

One of the most relevant interaction processes of radiation with matter is **absorption** by photochemical reactions, especially those that are part of the ozone destruction-creation cycle (Velázquez, 2001) [9]. The most energetic UV radiation is completely absorbed in these processes, so that only the longest wavelengths of the UV spectrum reach the earth's surface (∼280-400nm).

The **Rayleigh scattering** is an elastic scattering of light or electromagnetic radiation towards any direction different to the incident direction, i.e., without a change in its wavelength. It occurs when the electric fields of said radiation interact with those of molecules they encounter on their way (Zhao and Hiroyasu, 1993) [10]. The only wavelength change in this process, therefore, is due to the Doppler effect associated with the scattering of a moving target (Robben, 1975) [11].

The scattering differential angular section, σ_{ri}, specific to each particle, is defined as the scattered power per unit solid angle (intensity) divided by the linearly polarized incident power per unit area (irradiance), with units of cm^2/sr. The intensity of the radiation scattered by Rayleigh scattering is proportional to the integral sum at all angles (that is, the total cross section, which has surface units) and depends inversely on the fourth power of the wavelength of the radiation, so that the relation can be concluded:

$$I_r \propto \sigma_{ri} \propto \lambda^{-4} \tag{1}$$

Nevertheless, Rayleigh's theory is only valid as long as the wavelength of light is much larger than a characteristic size of scatterer particles, such as their diameter. According to Kerker [12], for the validity of the theory, this relation must be such that $d/(2\lambda) < 0.05$. Therefore, in the atmosphere, Rayleigh scattering occurs when sunlight hits atmospheric gases, which is why it is sometimes also known as molecular scattering.

On the other hand, scattering caused by particles

larger than Rayleigh scatters, i.e., with diameters greater than one tenth of the wavelength of incident radiation, is known as **Mie scattering** (McCartney, 1976) [13]. This scattering has no size limitations and can be applied to scattering caused by aerosols and cloud particles (Mateos, 2012) [8].

1.2. UV radiation. Components and types

For all these reasons, the radiation reaching the surface (*global radiation*) can be expressed as the sum of two components: *direct radiation* or *beam*, it being the one that reaches us with the direction of the SZA and the solar azimuth (i.e., the angle that indicates the direction of the Sun according to the cardinal points); and *diffuse radiation*, which represents radiation that has been scattered by the atmosphere and reaches the surface from any different direction.

Moreover, within UV radiation, three bands are defined according to the World Health Organization, depending on its wavelength (WHO, 2003) [4]:

- 100-280 nm ⇒ UV-C radiation: the most energetic, and therefore harmful, although it does not really pose a danger since it is absorbed entirely by atmospheric gases, in particular ozone in the lower stratosphere, located between 12 and 35 km altitude, and does not reach the Earth's surface. Even if this ozone was greatly reduced, all UV-C would still be completely absorbed (Calbò et. al, 2005) [14].
- 280-315 nm ⇒ UV-B radiation: less energetic than the previous one, it is only partially absorbed and scattered by the atmosphere, so it is the highest frequency (and therefore, most energetic) radiation that reaches the surface.
- 315-400 nm ⇒ UV-A radiation: which passes through the ozone layer with ease, being useful, e.g., in the synthesis of vitamin D by the body. Although, despite being the least energy, with effects of the order of a thousand times less than those of UV-B, prolonged exposure can also produce harmful effects on living organisms.

The aforementioned absorption and scattering phenomena cause UV radiation at the Earth's surface, made up of UV-A and UV-B, to correspond to only 7.45% of the incident solar radiation in the outermost layer of the atmosphere. (Fröhlich and London, 1986) [15]

The main aim of this study is to analyze and quantify the impact that the presence of clouds and aerosols in the atmosphere has on the amount of solar UV radiation that reaches the surface of our planet.

To achieve this, a series of statistical checks are run with the experimental data to validate the available clear sky model, and once its usefulness is certified, it will be used to compare these simulations with the measurements of radiation arrivals under different cloudy skies taken in the city of Granada between 2008 and 2012.

Afterwards, a study is developed on the dependence of a characteristic parameter of clouds and aerosols named Cloud/Aerosol Modification Factor (CMF/AMF) with wavelength, the measured quantities of clouds and aerosols present (taking oktas and AOD, respectively, as measures of those quantities) and geo-temporal parametres such as solar zenith angle (SZA).

2. Dependence on cloudiness

One of the main factors that control UV radiation levels, and the object of this study, is the cloudiness of the sky. Clouds are masses made up of microscopic ice crystals or water droplets suspended in the atmosphere. They are normally formed by condensation of moisture into particles and may therefore present a not necessarily homogeneous distribution in the sky. Furthermore, its presence is highly variable both in time and space.

Clouds scatter incident radiation through Mie scattering, which occurs when light strikes large particles or molecules (larger than the wavelength hitting on them); absorbing part of the light and reflecting the rest, giving the clouds a light color when they are –for the sake of redundancy– light, and turning dark when they are thick or the at-

mosphere is highly charged, accentuating the Mie effect.

It can be –correctly– thought, then, that the presence of clouds attenuates surface UV radiation, as it is the majority of times. However, the influence of clouds can sometimes be in such way that the radiation on the surface is greater than that which would arrive in clear sky conditions, according to studies such as Estupiñán et al. (1996) [16] or Schafer et al. (1996) [17], which measured some increases of up to 11 % UV-B transmission, phenomenon known as the "enhancement effect".

Given the usual heterogeneity of the distribution of clouds across the sky, *oktas*, which measure cloud cover in eighths of covered sky, are the main unit in which cloud cover measurements are taken. Thus, if we divide sky into 8 parts, the number of them covered by clouds is represented by an integer, which means that a completely cloudy sky is equivalent to 8 oktas and a totally clear one to 0 oktas.

The parameter used to describe the effects of clouds on radiation is known as the Cloud Modification Factor (CMF), defined as follows:

$$CMF = \frac{UV_{meas}}{UV_{clear}} \tag{2}$$

where UV_{meas} is radiation measured under any cloudy condition and UV_{clear} that same radiation measured under the very same atmospheric conditions but with a clear sky, eliminating the effect of clouds. These UV amounts are usually weighted erythemal irradiances, although they can be other unweighted UV values. This quotient has the physical meaning of transmittance of clouds in a given spectral interval.

So, we are able to compare and estimate, using clear sky simulations, the enhancing or diminishing effect of clouds on incident radiation.

3. Dependence on the amount of aerosols

Aerosols can be defined as a suspension of solid or liquid particles in a gaseous medium (Toledano, 2005) [18], and their size in our atmosphere varies from thousandths of a micron to 100µm (Román, 2012) [7].

They can be produced by reactions or physical and chemical processes in the atmosphere itself or be ejected into it both by human activity or naturally (e.g.: haze, which is suspended desert dust; smoke from fires or volcanic ash) and will be able to scatter (by Mie scattering, see section 1.1) and absorb (although not as selectively as gases) part of the solar radiation in the atmosphere. When a photon hits an aerosol particle, if it is absorbed or redirected by scattering, we speak of an "extinction" phenomenon.

For the treatment of the aerosol effect, the aerosol optical depth by extinction, AOD, is usually used. It will be the sum of the absorption aerosol optical depth (AAOD) and the scattering aerosol optical depth (SAOD), related respectively to the probability that a photon that incides perpendicularly to the Earth's surface undergoes an absorption, or a scattering phenomenon, by the amount of aerosol present on the surface.

In this way, the AOD is in turn related to the possibility that the photon undergoes extinction, which is represented by the Beer-Bouguer-Lambert law:

$$\frac{I_{dir\lambda}}{I_{0\lambda}} = e^{-m_\lambda \tau_\lambda} \tag{3}$$

where I_{dir} is the direct irradiance measured at ground level, I_0 is the extraterrestrial irradiance, corrected for Earth-Sun distance; m is the relative optical mass, which is defined as the ratio of the mass of air passing through the radiation in the incident direction to that which would pass through if the incidence were vertical to the ground; and τ is the total atmospheric optical depth, i.e. the sum of all contributions of Rayleigh ($\tau_{r\lambda}$), ozone absorption ($\tau_{o\lambda}$), water vapour ($\tau_{w\lambda}$), atmospheric

gases ($\tau_{g\lambda}$) and aerosol ($\tau_{a\lambda}$) optical depths as defined in (4):

$$\tau_\lambda = \tau_{a\lambda} + \tau_{r\lambda} + \tau_{o\lambda} + \tau_{w\lambda} + \tau_{g\lambda} \tag{4}$$

In the solar range, the AOD itself, written indistinctly as $\tau_{a\lambda}$, varies empirically with the wavelength of the radiation, following Ångström's formula (Ångström, 1963):

$$\tau_{a\lambda} = \frac{\beta}{\lambda^\alpha} \tag{5}$$

where the Ångström exponent, α, is related to the size distribution of the aerosol, taking larger values the smaller the particles, always in the range 0 - 4; and the turbidity coefficient, β, corresponds to the value of the AOD for a wavelength of 1 μm. Both are dimensionless while λ is taken in μm.

In Figure 1 the dependence of the spectral AOD for different values of the coefficients α and β in the range of UV reaching the surface is shown.

Numerous authors have reported the effects of aerosols on surface radiative levels. Among them, *Román et. al* (2012) found that for a wavelength of 440nm, EUVR (erythemal ultraviolet radiation) levels decrease by, on average, 28.4% per unit AOD [19]. *Marín et al.* (2007) observed that for $\lambda = 550$ nm, the change of an aerosol optical depth from 0.1 to 0.3, caused the EUVR to drop by 14% to 20%, as well as by 13% to 19% when increasing from 0.3 to 0.5, with the largest decrease corresponding to winter and the smallest to summer [20].

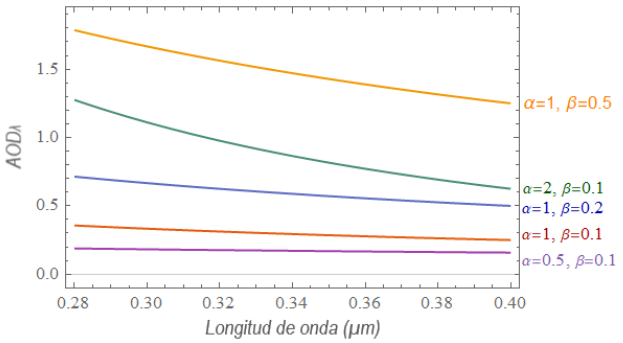

Figure 1: *Variation of the AOD with* λ *as a function of the parameters* α *and* β

The parameter used to describe the effects of aerosols on radiation is known as the Aerosol Modification Factor (AMF), defined as follows:

$$AMF = \frac{UV_{clear-meas}}{UV_{clear-noaerosol}} \tag{6}$$

where $\mathrm{UV}_{clear-meas}$ is radiation measured under clear-sky condition and $\mathrm{UV}_{clear-noaerosol}$ that same radiation measured under the very same atmospheric conditions but with no present aerosol, eliminating the effect of clouds. Like in CMF (2), these UV amounts are usually weighted erythemal irradiances, although they can be other unweighted UV values. This quotient has the physical meaning of transmittance of aerosols in a given spectral interval.

So, we are able to compare and estimate, using clear sky without aerosols simulations, the enhancing or diminishing effect of aerosols on incident radiation.

4. Data

4.1. Measuring station and instrumentation

The station of the Atmospheric Physics Group (GFAT) of the University of Granada is placed on the rooftop of the Andalusian Center for Environmental Studies (CEAMA, located in Granada, Spain, at latitude 37.16°N and longitude 3.6°W, 680 m above sea level), collecting meteorological and radiometric information through broadband radiometers in all regions of the spectrum: UV,

visible and IR; a photometer (CIMEL CE318) and a Bentham DMc-150 spectroradiometer.

This spectroradiometer consists of a double monochromator with a robotic mirror to be able to receive inputs from two different light sources. At its exit, a photomultiplier tube (R1527 Hamamatsu) is installed, that records the scattered UV light, with a blue filter on the detector to prevent visible wavelengths from reaching it. The monochromator altogether with the detector are in a container at a temperature of 25°C, stabilized by an air/air Peltier cell refrigerator system. The monochromator input is connected to two diffusers located on the roof of CEAMA by means of two optical fibers (LI-J1010), so that direct radiation measurements can be taken in one of them and global and diffuse in the other. We will refer in this study to the set of monochromator, detector and diffusers (with the optical fibers) as *Bentham spectroradiometer*.

The diffuser in charge of measuring the direct component of the irradiance achieved its purpose by means of a collimator tube with three optical diaphragms and a field of view of 1.2°, placed on a solar tracker with precise aiming –better than 0.02°– thanks to a solar sensor (model 2AP by Kipp and Zonen) that guarantees that the tube is always pointing to the solar disk (Antón et al., 2013) [21]. Next to it, the other diffuser, took the global irradiance measurements and also the diffuse ones, helped by a rotating shadow band.

The instrument takes measurements every 15 minutes of all of them in the interval between 280 and 400 nm, with steps of 0.5 nm. It takes approximately 4 minutes (one second for each wavelength measured) to take a full spectrum of global radiation, time after which spectra of direct and diffuse radiation are taken.

Meanwhile, the optical depth of aerosols and the Angström exponent are obtained from direct solar irradiance measurements taken by a CIMEL CE-318 solar photometer located next to the Bentham spectroradiometer, at 340, 380, 440, 500, 670, 870 and 1020 nm (Román et al., 2013) [22]. These data were obtained directly from the AERONET network, using data from version 3.

The okta data analyzed here were automatically taken using the ASI camera in Granada and manually revised after, due to some algorithm problems in high haze conditions (Saharan dust in suspension), where sometimes the algorithm classified the sky as having a high cloud cover, due to its whitish color in the presence of dust, despite being clear of clouds (Cazorla, 2008) [23].

4.2. Measures and model used

Between 2008 and 2012, spectral UV radiation data were taken in the city of Granada with the aforementioned Bentham spectroradiometer. They were used for this study, along with clear sky simulations which allowed us to compare and analyze the dependence on the clouds that control the arrival of UV on Earth.

These data contain for each recorded measurement (one every 15 minutes) values of global irradiance, G, direct irradiance measured in the normal direction to Sun, B *(beam)*, and direct irradiance on the horizontal surface, D, obtained according to $D = B\,cos(SZA)$. For each of these types of measurements, irradiance values were obtained in mW/m^2 for each wavelength between 280 and 400 nm, with steps of 0.5 nm.

These were, in each case, complemented with data from the SZA, cloud cover in oktas (provided by the ASI sky camera); daily ozone column in Dobson units (DU) measured by satellite (Ozone Monitoring Instrument, OMI, aboard the spacecraft Aura), and aerosols instantaneous and daily aerosol properties like AOD at 340, 380 and 440 nm for each measurement, as well as its daily average; and the Ångström exponent, α (from the AERONET [24] network), as well as the daily average of the values measured during the day.

In addition, a model is available with simulated values under cloudless skies for global, direct and diffuse radiation. These simulations were carried out with the radiative transfer model *LibRadtran* [25], using ozone, aerosols (AOD and Ångström exponent) and geo-temporal parameters (SZA and Earth-Sun distance) as input parameters.

This work was focused on the analysis of global radiation as well as its components (beam and diffuse) alone. Diffuse irradiance was calculated from the spectroradiometer's measurements as it follows:

$$I_{Dif} = G - D \tag{7}$$

Since beam irradiance measurements are taken 5 minutes later than global, this lead to some negative values appearing on the calculation of diffuse radiation data, because of direct irradiance being higher than the global measured 5 minutes earlier. These values were filtered so they don't alter the mean values obtained later.

5. Model validation

From the measured global UV radiation data and their corresponding clear sky simulations, spectra such as the one shown as an example in Figure 2 could be obtained, where it can be observed at first sight that these simulated data are very much related to the ones measured.

For the statistical analysis, the 'absolute' mean error (MBE), root mean square error (RMSE) and standard deviation (STD) parameters were spectrally calculated (both with irradiance units mW/m^2, and in %) and are shown in Figure 3.

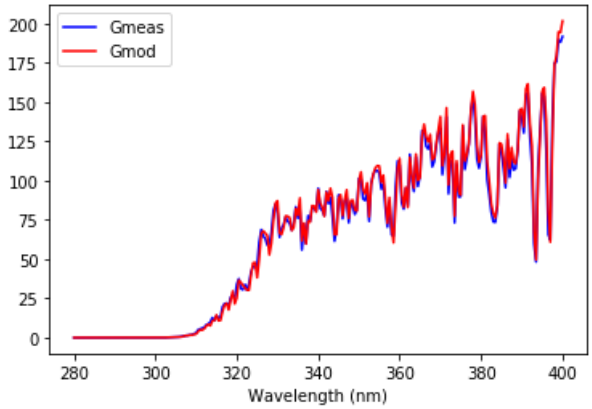

Figure 2: *Irradiance data measured (blue) and modeled (red) for global radiation on October 30, 2008, at 9:00 a.m., with a measurement of 0 oktas and an SZA of 66.021°*

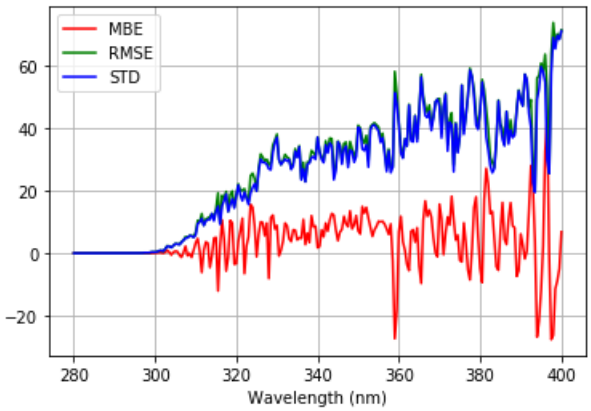

(a) Statistical parameters in units of mW/m^2.

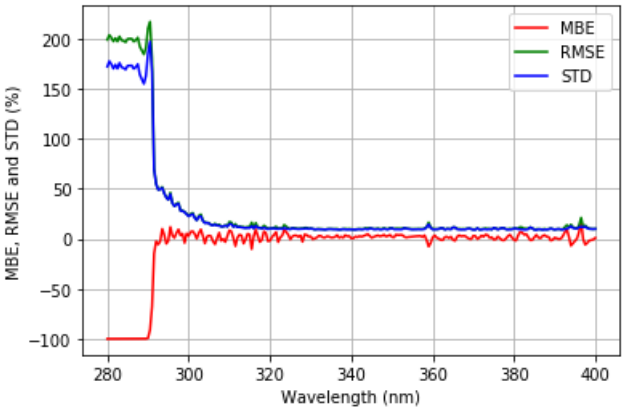

(b) Relative statistical parameters (in %).

Figure 3: *Spectral representation of the absolute and relative statistical parameters of the model-measurement comparison for global radiation*

Finally, the coefficient of determination r^2 was obtained along the wavelengths of study and, to complement this representation, the slope and intercept were calculated from a linear fit of all data using the method of least squares (measured versus modeled values), regardless of the wavelength at which each pair was taken.

Regarding the lineal fit, a value for the slope of 0.9766 and for the intercept of 9.979 mW/m^2 was obtained. The r^2 coefficient of all these data is 0.9822.

The same study was run for the direct component, obtaining the results shown in Figure 4. In this case, the value obtained for the slope from the lineal fit was 0.8861; and for the intercept, 19.2180 mW/m^2. The r^2 coefficient of all these data is 0.8923.

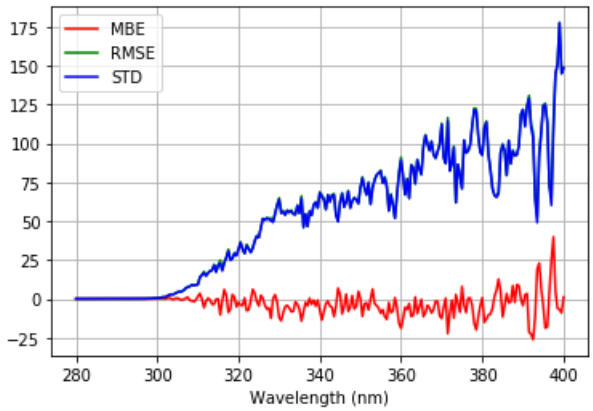

(a) Statistical parameters in units of mW/m^2.

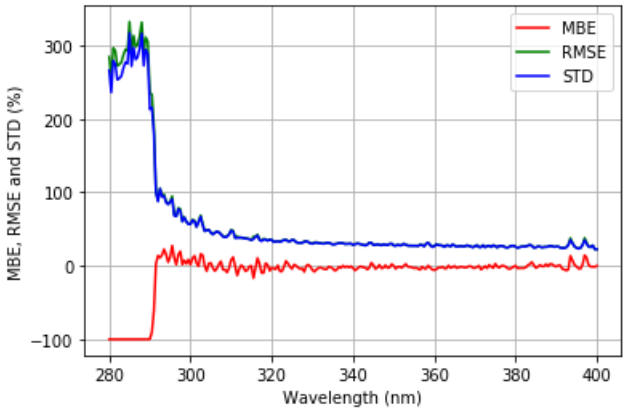

(b) Relative statistical parameters (in %).

Figure 4: *Spectral representation of the absolute and relative statistical parameters of the model-measurement comparison for direct radiation*

As aforementioned, it can be graphically observed in the particular example of Figure 2 the apparently good correlation between measured and modeled data of UV radiation, in this situation of clear or almost cloudless skies. Said correlation is quantified by adjusting the measures against the simulated values using least squares, being better the closer the slope of the fit is to 1 and the intercept to 0.

In the two cases studied, slope values close to 1 are observed, with the value obtained with the global radiation data (0.9766) being closer than the direct one (0.8861). The closest to 0 value of the intercept (9.979 mW/m^2) is also given for global radiation, compared to direct radiation (19.2180 mW/m^2).

These values of the intercepts are perhaps a little distant from 0, especially in the case of direct radiation, which is about 19 mW/m^2, when the measured data took values up to 700-800 mW/m^2, an error of $\approx 2.5\%$. In the case of the global one, the intercept value of something less than 10 mW/m^2 is more negligible compared to the data used, constituting an error of $\approx 1.5\%$).

In addition, the value of the coefficient of determination r^2 is close to 1 in both cases, although it is, once again, higher in global radiation (0.9822, implying a very high correlation) than in direct (0.8923, high correlation). The differences between the values that mark a perfect correlation ($r^2 = 1$) and those obtained account for the uncertainty in the simulation of the data.

Regarding the statistical parameters, MBE takes absolute values between -20 and +20 mW/m^2 for global radiation, while for direct radiation these values are even lower. As these values are always around zero, it can be concluded that the model does not overestimate (MBE > 0) or underestimate (MBE < 0) the measurements, thus presenting high accuracy. On the other hand, the standard deviation (STD), which gives an idea of the uncertainty of the model, takes relative values of around 10% for global radiation and between 20 and 30% for direct radiation.

It is also observed that the relative values of the MBE and RSME, as well as the standard deviation, reach maximums well above the rest of the values for short wavelengths (280-300nm), which are reached when the absolute values are are close to 0, since they have a greater sensitivity to changes in values and situations close to 0/0 can be incurred in the calculations.

Finally, it should be noted that the measured irradiance begins to have non-negligible values from 300-310 nm, for global radiation, and about 320 nm for the direct component. Said irradiance, in the UV range, increases as the wavelength increases, and so do the MBE, RMSE and standard deviation parameters, in addition to slightly decreasing the correlation coefficient, r, due to the increasingly variant data that we have.

Taken all of this into consideration, we can conclude that the model is valid for our purpose, and so was used to calculate the CMF for both global and direct radiation.

Moreover, it must be noted that, even though it is not directly proven, since the model is valid for both global and direct (beam) radiation, it will as well be valid for diffuse radiation (as it is obtained from the other two, according to (7))

6. Results: Effect of clouds

6.1. Global radiation

The measured irradiance starts having non-negligible values at 300-310 nm, in the case of global radiation, as can be seen in Figure 2. After representing the CMF (according to equation (2)) in the study range (280-400 nm), the data of the shorter wavelengths will be neglected, since hardly any irradiance reaches and in which the calculation of the CMF does not provide consistent results.

The CMF for the remaining wavelengths (300-400nm) is represented in Figure 5, where the different possible oktas values have been classified into four descriptions of the cloudiness of the sky:

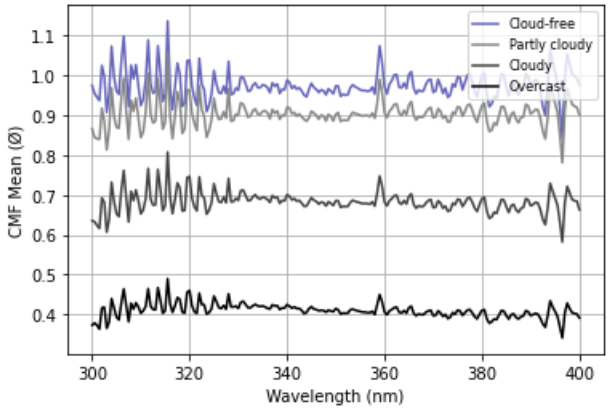

Figure 5: *CMF as a function of wavelength and sky cloudiness for global radiation*

The mean value of the CMF in this interval as well as it standard deviation (SD), obtained under the different sky covers and SZA ranges taken for global radiation, is shown below, in Table 1:

Table 1: *Mean values of CMF_G and SD as a function of SZA and sky cloudiness*

Cover	SZA	CMF_G	
		CMF	*±SD*
Cloud free (0 - 2 oktas)	15°	0,9982	0,0905
	35°	0,9939	0,0941
	55°	0,9685	0,0996
	75°	0,9665	0,1098
	ANY	0,9757	**0,1007**
Partly Cloudy (3 - 5 oktas)	15°	0,9630	0,1552
	35°	0,9276	0,1850
	55°	0,8920	0,1803
	75°	0,8803	0,1597
	ANY	**0,9038**	**0,1736**
Cloudy (6 - 7 oktas)	15°	0,6972	0,2716
	35°	0,6922	0,2775
	55°	0,6750	0,2506
	75°	0,6823	0,2351
	ANY	**0,6827**	**0,2534**
Overcast (8 oktas)	15°	0,5369	0,2768
	35°	0,4229	0,2572
	55°	0,3899	0,2265
	75°	0,4044	0,2279
	ANY	**0,4099**	**0,2357**
TOTAL		**0,8460**	**0,1513**

Furthermore, it is interesting to analyze the impact of SZA on global irradiance, and see how it is extinguished depending on the angle of incidence.

For that purpose, 4 different ranges of SZA have been studied: 0-25° (marked from now on as "SZA = 15°"), 25°-45° (35°), 45°-65° (55°), and 65°-85° (75°), with any SZA greater than 85° being discarded.

Figures 6 to 8 show the spectral dependence of CMF for every one of these ranges, as well as its SD displayed as a shadow band.

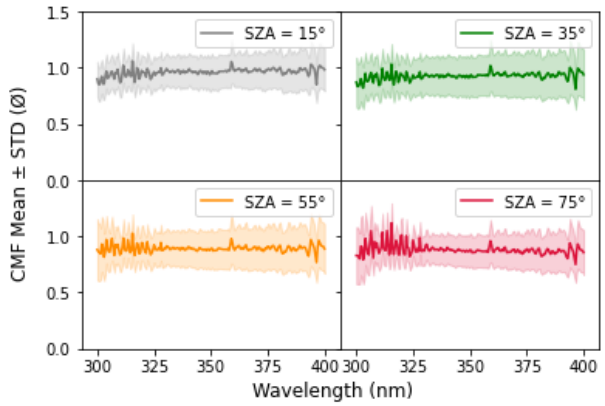

Figure 6: *CMF_G as a function of λ and SZA under partly cloudy conditions (3-5 oktas)*

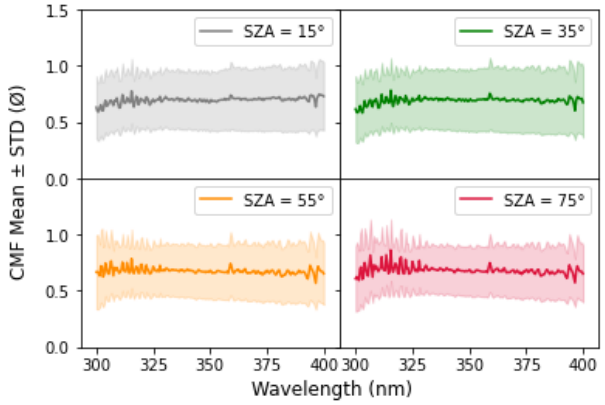

Figure 7: *CMF_G as a function of λ and SZA under cloudy conditions (6-7 oktas)*

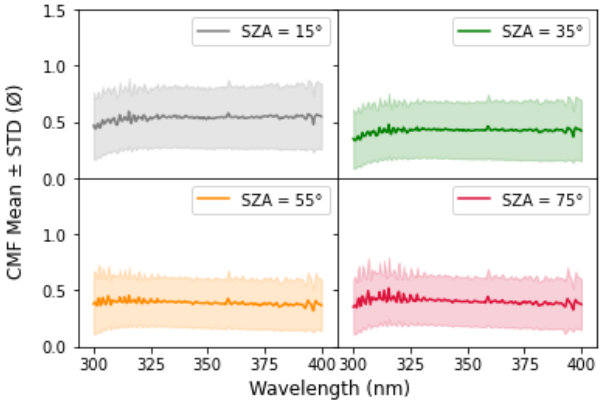

Figure 8: *CMF_G as a function of λ and SZA under overcast conditions (8 oktas)*

6.2. Direct radiation

In the case of the direct component, the measured irradiance starts having non-negligible values from 310-320 nm. CMF is represented in the study range, and the data of the shorter lengths are neglected, of which hardly any irradiance reaches.

Also, to avoid situations where there is barely any irradiance, causing the CMF to take anomalously high values (the quotient approaches a 0/0-esque indetermination), any CMF obtained higher than 3 has been filtered out of the calculation of mean and spectral CMF.

The CMF for the remaining wavelengths (310-400nm) is represented in Figure 9, where the different levels of possible octas have been classified into four descriptions of the cloudiness of the sky:

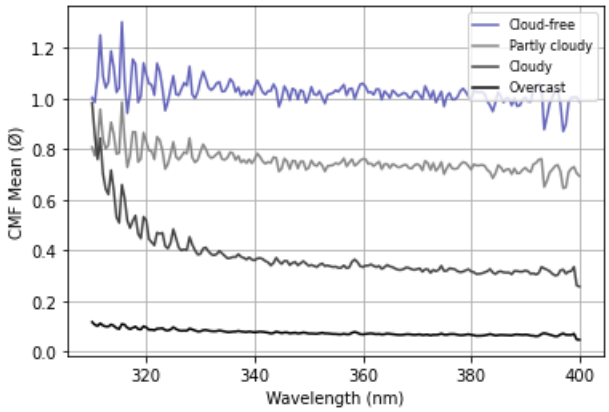

Figure 9: *CMF as a function of wavelength and sky cloudiness for beam radiation*

Finally, Table 2 shows the mean value of the CMF calculated in the interval 320-400 nm (in order to avoid the harsh decrease of the CMF with the wavelength observed up to 320 nm for cloudy skies), as well as its SD, obtained under different sky covers and SZA for direct radiation:

Table 2: *Mean values of CMF_B and SD as a function of SZA and sky cloudiness*

Cover	SZA	CMF_B	
		CMF	*±SD*
Cloud free (0 - 2 oktas)	15°	1,0142	0,2643
	35°	1,0024	0,2479
	55°	0,9975	0,2167
	75°	1,0556	0,3493
	ANY	**1,0167**	**0,2657**
Partly Cloudy (3 - 5 oktas)	15°	0,8458	0,3387
	35°	0,7807	0,3736
	55°	0,6896	0,3993
	75°	0,6232	0,4940
	ANY	**0,7030**	**0,4161**
Cloudy (6 - 7 oktas)	15°	0,3895	0,4169
	35°	0,3164	0,3885
	55°	0,2478	0,3501
	75°	0,2017	0,3587
	ANY	**0,2610**	**0,3664**
Overcast (8 oktas)	15°	0,1657	0,2884
	35°	0,0895	0,2136
	55°	0,0338	0,1237
	75°	0,0253	0,1129
	ANY	**0,0542**	**0,1536**
TOTAL		**0,7328**	**0,2850**

Figures 10 - 12 shows the spectral behavior of CMF in four different SZA ranges, under more and less cloudy skies. The shadow represents the standard deviation (SD) of the data. Clear skies are not shown since the possible mitigating or enhancing effect of clouds is assumed trivial.

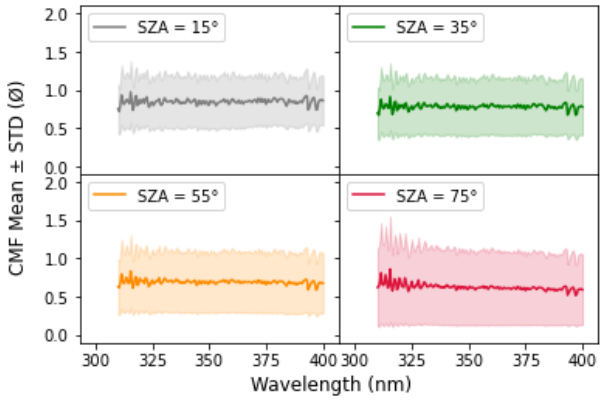

Figure 10: *CMF_B as a function of λ and SZA under partly cloudy conditions (3-5 oktas)*

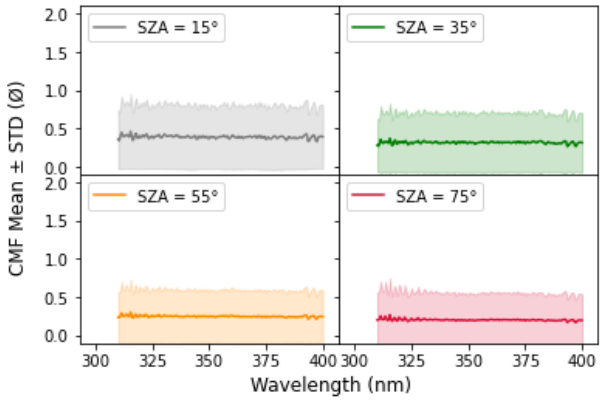

Figure 11: *CMF_B as a function of λ and SZA under cloudy conditions (6-7 oktas)*

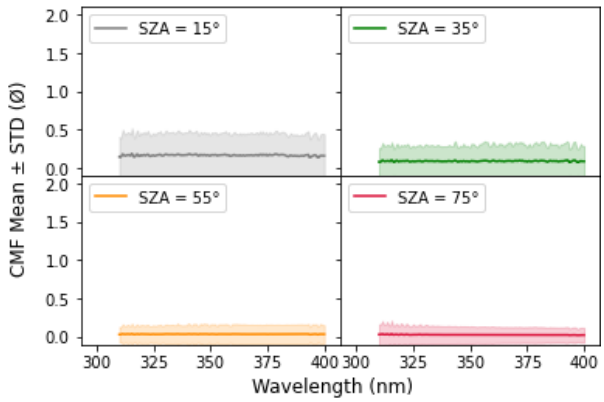

Figure 12: *CMF_B as a function of λ and SZA under overcast conditions (8 oktas)*

6.3. Diffuse radiation

Let us consider now diffuse radiation. Since there was some radiation at 300-310 nm, and almost none of it was beam radiation, we must assume that it was indeed diffuse irradiance that reaches the Earth with wavelengths within the range of 300-400nm, as represented in figure 13. Once again, the cloudiness of the sky has been categorised into 4 different levels of cloud cover.

The mean values of the CMF, along with their SD, calculated in the interval 300-400nm under different sky covers and SZA for diffuse radiation are displayed on Table 3:

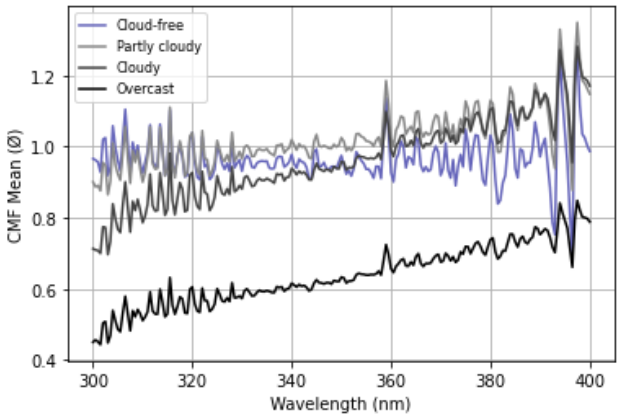

Figure 13: *CMF_{Dif} as a function of wavelength and sky cloudiness*

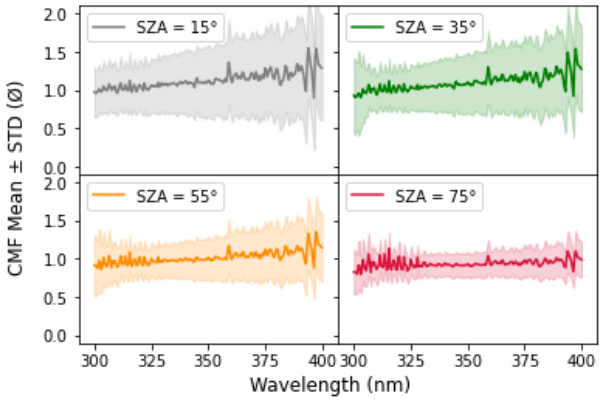

Figure 14: *CMF_{Dif} as a function of λ and SZA under partly cloudy conditions (3-5 oktas)*

Table 3: *Mean values of CMF_{Dif} and SD as a function of SZA and sky cloudiness*

Cover	SZA	CMF_Dif	
		CMF	*±SD*
Cloud free (0 - 2 oktas)	15°	1,0015	0,3918
	35°	1,0025	0,3194
	55°	0,9521	0,1879
	75°	0,9519	0,1372
	ANY	0,9672	0,2194
Partly Cloudy (3 - 5 oktas)	15°	1,1251	0,4652
	35°	1,0970	0,4018
	55°	1,0163	0,3021
	75°	0,9348	0,1882
	ANY	**1,0255**	**0,3125**
Cloudy (6 - 7 oktas)	15°	1,1252	0,5141
	35°	1,1148	0,5152
	55°	0,9640	0,3553
	75°	0,7899	0,2615
	ANY	**0,9635**	**0,3795**
Overcast (8 oktas)	15°	1,0145	0,4741
	35°	0,7951	0,4375
	55°	0,6165	0,3371
	75°	0,4879	0,2660
	ANY	**0,6364**	**0,3429**
TOTAL		**0,9297**	**0,2721**

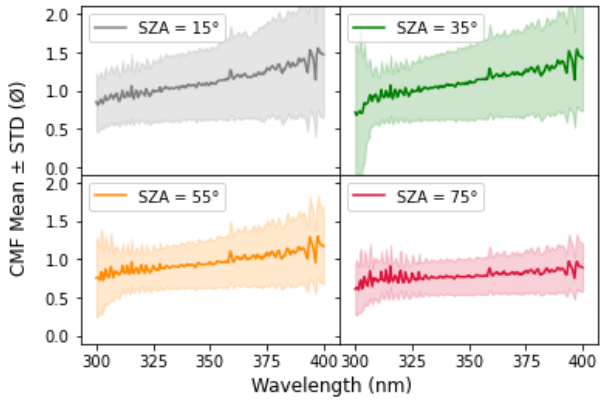

Figure 15: *CMF_{Dif} as a function of λ and SZA under cloudy conditions (6-7 oktas)*

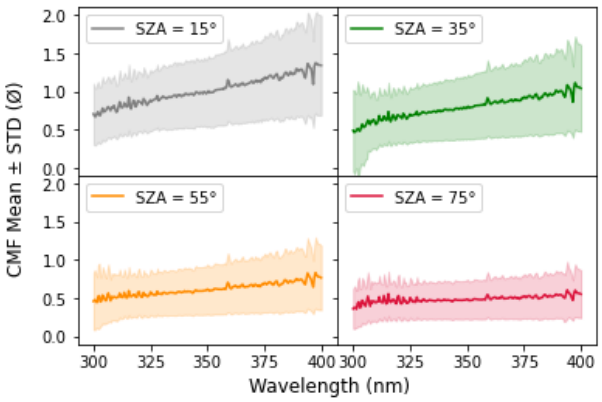

Figure 16: *CMF_{Dif} as a function of λ and SZA under overcast conditions (8 oktas)*

Figures 14 - 16 show the spectral behavior of CMF (± SD) in different SZA ranges, under different cloud covers, with the 'clear sky' case again not being shown because of the possible mitigating or enhancing effect of clouds being assumed trivial.

7. Results: Effect of aerosols

Following a scheme similar to that of the previous section, here it is shown the results of the study of the effect of aerosols on solar UV radiation. In this case, the Aerosol Modification Factor (AMF, defined in (6)) is used as the main parameter. Since our model is proven valid, we can compare the irradiance measured by the spectroradiometer under clear-sky conditions to those simulated values under the same atmospheric conditions (that includes, of course, clear sky) and no aerosol (we will consider AOD $<$ 0.1).

Different ranges of AOD will be taken into consideration to note the greater or lesser effect aerosols have when they ae present in a different quantity. These ranges will be: AOD smaller than 0.1 , AOD = 0.1 - 0.25, AOD = 0.25 - 0.4 and AOD greater than 0.4.

It must be noted that the case AOD $<$ 0.1 is often disregarded in this study, as it really is similar to an aerosol-free condition, take the case of the first panel in Figure 17 where values that AMF takes are very near to 1 and therefore meaning that the aerosols have almost no effect on radiation extinction.

Also, to avoid situations where there is barely any irradiance, causing the AMF to take anomalously high values (the quotient approaches a 0/0-esque indetermination), any AMF obtained higher than 3 has been filtered out of the calculation of mean and spectral AMF.

At last, the dependence on SZA will also be calculated, using the same SZA ranges as in section 6.

7.1. Global radiation

As it was discussed in section 6.1, in the case of global radiation measured irradiance starts having non-negligible values at 300-310 nm. AMF was represented along wavelengths of 300-400 nm in Figure 17. Each panel shows a different aerosol presence, e.g. the AOD ranges mentioned before, and is plotted together with its SD as a shadow band.

The mean values of AMF in each AOD range as well as its standard deviation (SD), obtained for global radiation for the SZA ranges taken, are shown below, Figures 18 - 20 and Table 4:

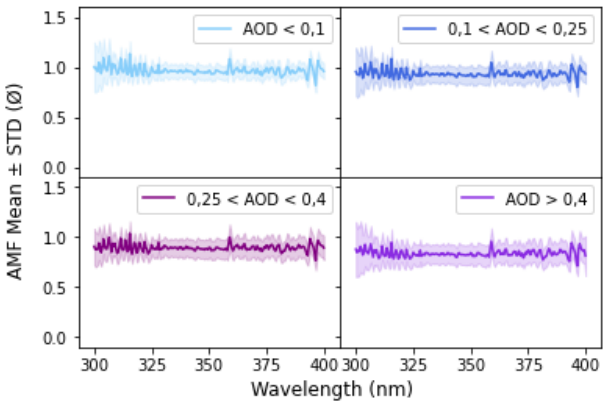

Figure 17: *AMF_G as a function of λ and AOD*

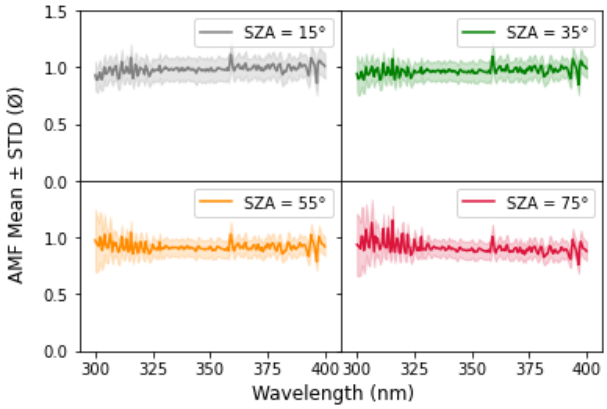

Figure 18: *Spectral AMF_G as a function of AOD and SZA under partly cloudy conditions*

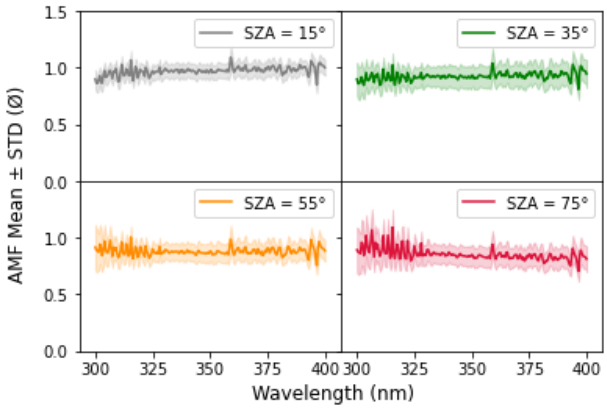

Figure 19: *Spectral AMF_G as a function of AOD and SZA under cloudy conditions*

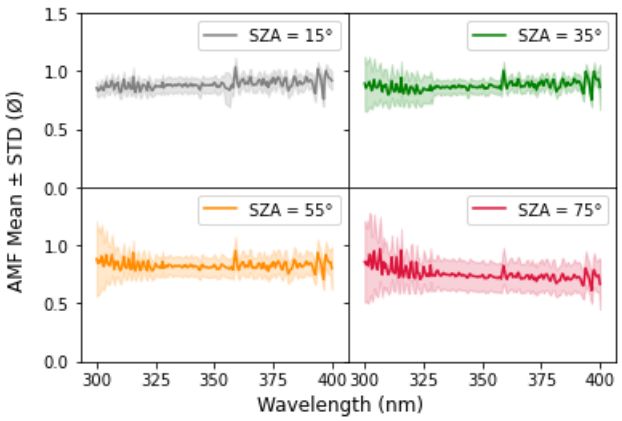

Figure 20: *Spectral AMF_G as a function of AOD and SZA under overcast conditions*

Table 4: *Mean values of AMF_G and SD as a function of SZA and AOD*

AOD	SZA	AMF_G	
		AMF	*±SD*
AOD < 0.1	15°	0,9957	0,0877
	35°	0,9967	0,0942
	55°	0,9596	0,0748
	75°	0,9575	0,0856
	ANY	**0,9659**	**0,0821**
0.1 < AOD < 0.25	15°	0,9859	0,1024
	35°	0,9702	0,0910
	55°	0,9172	0,0900
	75°	0,9089	0,0935
	ANY	**0,9325**	**0,0921**
0.25 < AOD < 0.4	15°	0,9734	0,0683
	35°	0,9266	0,1015
	55°	0,8801	0,0899
	75°	0,8536	0,1035
	ANY	**0,8930**	**0,0945**
AOD > 0.4	15°	0,8881	0,0684
	35°	0,8743	0,0851
	55°	0,8276	0,1033
	75°	0,7520	0,1473
	ANY	**0,8361**	**0,1010**
TOTAL		**0,9298**	**0,0911**

7.2. Direct radiation

As aforementioned (section 6.2), the study range for direct radiation is a bit shorter (310-400 nm). AMF was represented along this range of wavelengths in Figure 25 where each panel shows a different quantity of aerosol, e.g. the AOD ranges we are treating with. The plots show mean AMFs together with their SD as a shadow band.

The mean value of the AMF in each AOD range as well as its standard deviation (SD), obtained for global radiation under the different SZA considered, is shown below, in Figures 22 - 24 and Table 5:

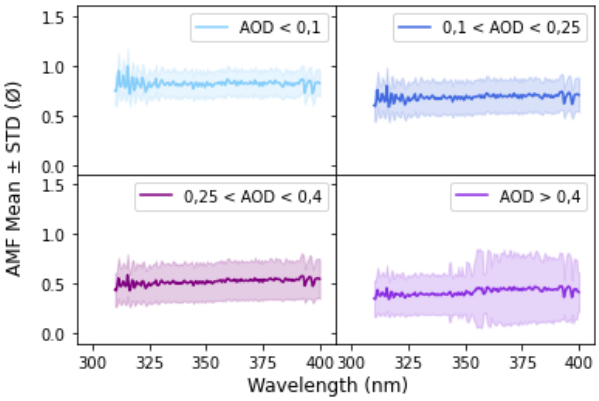

Figure 21: *AMF_B as a function of λ and AOD*

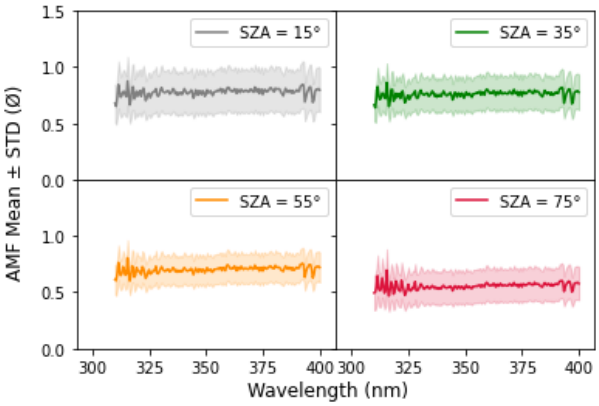

Figure 22: *Spectral AMF_B as a function of AOD and SZA under partly cloudy conditions*

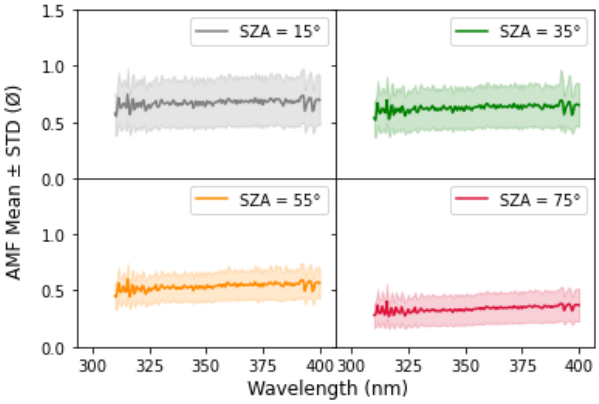

Figure 23: *Spectral AMF_B as a function of AOD and SZA under cloudy conditions*

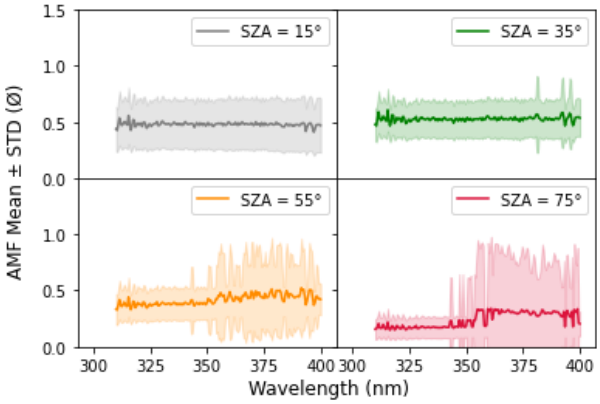

Figure 24: *Spectral AMF_B as a function of AOD and SZA under overcast conditions*

Table 5: *Mean values of AMF_B and SD as a function of SZA and AOD*

AOD	SZA	AMF_B	
		AMF	*±SD*
AOD < 0.1	15°	0,8532	0,1944
	35°	0,8311	0,1788
	55°	0,8397	0,0939
	75°	0,7728	0,1262
	ANY	**0,8149**	**0,1259**
0.1 < AOD < 0.25	15°	0,7794	0,1913
	35°	0,7607	0,1526
	55°	0,7006	0,1329
	75°	0,5537	0,1487
	ANY	**0,6805**	**0,1465**
0.25 < AOD < 0.4	15°	0,6724	0,2161
	35°	0,6274	0,1865
	55°	0,5371	0,1304
	75°	0,3362	0,1354
	ANY	**0,5222**	**0,1530**
AOD > 0.4	15°	0,4798	0,2262
	35°	0,5278	0,1728
	55°	0,4167	0,2344
	75°	0,2403	0,2945
	ANY	**0,4192**	**0,2291**
TOTAL		**0,6683**	**0,1463**

7.3. Diffuse radiation

Just like the other components, the dependence of AMF_{Dif} with wavelengths within the study range (in this case, 300-400 nm) was analyzed and the results were exposed in the current section.

Figure 25 shows AMF represented along this range of wavelengths where each panel shows a different quantity of aerosol, i.e. the AOD ranges we are treating with. Moreover, Figures 26 - 28 display the spectral variation of AMF_{Dif} when measured different aerosol types and its dependence on SZA. Table 6 contains the whole analysis of results obtained when SZA is taken into consideration.

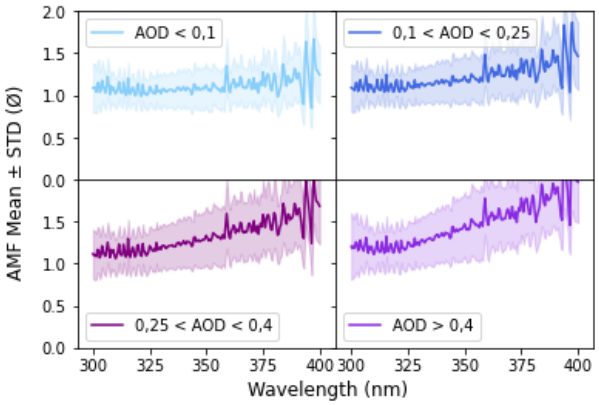

Figure 25: *AMF_{Dif} as a function of λ and AOD*

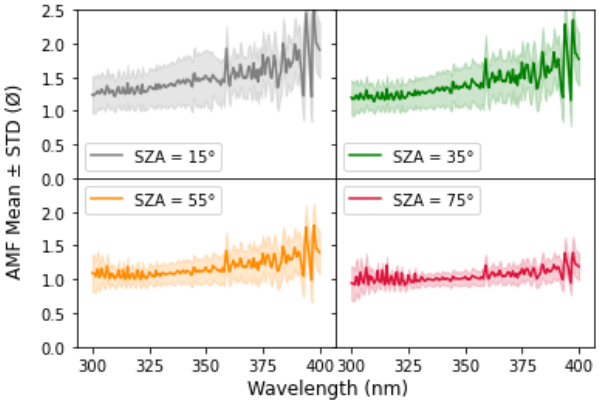

Figure 26: *Spectral AMF_{Dif} as a function of AOD and SZA under partly cloudy conditions*

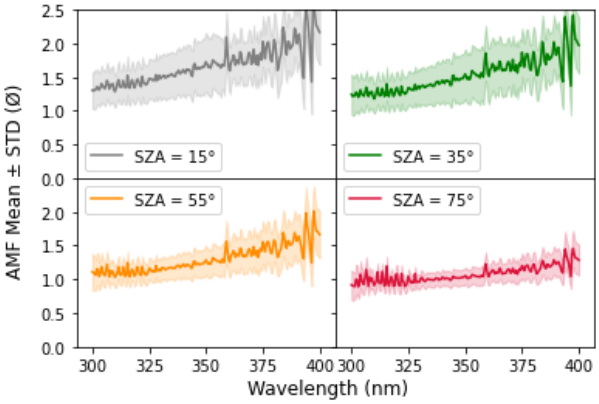

Figure 27: *Spectral AMF_{Dif} as a function of AOD and SZA under cloudy conditions*

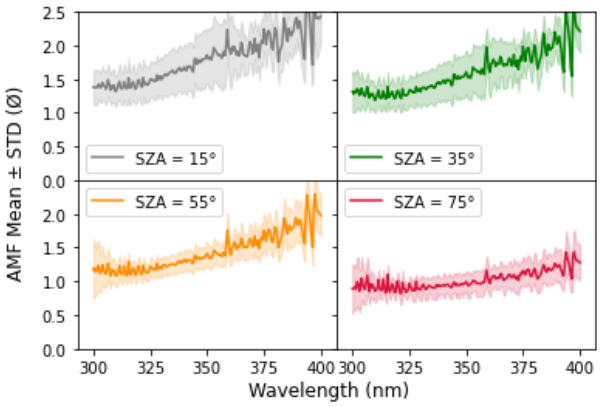

Figure 28: *Spectral AMF_{Dif} as a function of AOD and SZA under overcast conditions*

Table 6: *Mean values of AMF_{Dif} and SD as a function of SZA and AOD*

AOD	SZA	AMF_Dif	
		AMF	*±SD*
AOD < 0.1	15°	1,3418	0,3419
	35°	1,3318	0,2972
	55°	1,0808	0,1832
	75°	1,0208	0,1267
	ANY	**1,1165**	**0,1920**
0.1 < AOD < 0.25	15°	1,4970	0,3257
	35°	1,4093	0,2808
	55°	1,1763	0,2138
	75°	1,0510	0,1341
	ANY	**1,2238**	**0,2172**
0.25 < AOD < 0.4	15°	1,6612	0,3529
	35°	1,5234	0,3305
	55°	1,3002	0,2350
	75°	1,0718	0,1496
	ANY	**1,3320**	**0,2486**
AOD > 0.4	15°	1,7571	0,3397
	35°	1,5917	0,2741
	55°	1,4371	0,2026
	75°	1,0170	0,1911
	ANY	**1,4552**	**0,2442**
TOTAL		**1,2311**	**0,2193**

8. Discussion

- Comparing the direct radiation that reaches the ground under overcast skies (8 oktas), which is approximately only 5.42% of the radiation that would reach under a clear sky; with global radiation in the same case, which is around half (40.99%) of what it would reach if there were no clouds, it is obvious that clouds that completely cover the sky have attenuated, on average, the arrival of direct radiation by 94.58%, while only 59.01% of the total radiation.

  This indicates that, in the presence of many clouds, direct radiation decreases, while diffuse radiation increases or at least does not decrease as much, leading to global radiation not decreasing as much as direct radiation. This can be confirmed by looking at CMF_{Dif} results (Table 3): for overcast skies, 63.64% of diffuse radiation reaches the surface, which means a decrease of only 36.36%, and thus being the component of which a higher proportion touches the ground under a greatly dense cloud cover.

- For cloudy skies (between 6 and 7 oktas), clouds have a much smaller effect than in the previous case, reducing global radiation by 31.73%, and direct radiation by 73.90%; while for partly cloudy skies (between 3 and 5 oktas), clouds only attenuate an average of 9.62% of total radiation and up to 29.7% of direct radiation. For skies other than overcast, diffuse radiation stays around 1 which, taking into consideration the high error of these calculations (20 - 35%), could tell us that the incident radiation back-scattered by clouds may be in a way compensated with radiation that reaches the surface thanks to that scattering, as it would miss the ground otherwise.

- The analysis of clear skies is interesting, where the CMF is found to be greater for the direct component than for global radiation, even taking an average value greater than 1. These values not being exactly 1 can be explained when it is noted that the data of the model used, although precise, are not completely exact, in addition to the fact that the category of *clear skies* included skies of 0 oktas but also 1 and 2 oktas, with the presence of clouds (even if they were very few).

  It has been discarded that these values slightly greater than 1 obtained for the average CMF_B could be due to the enhancement effect, since

that additional 1.67% falls within the uncertainty of the model used. In addition, if there really was an enhancement effect, it would be better appreciated in the global than in the direct radiation.

- Nevertheless, we can say there was some kind of "enhancement effect" of aerosols on diffuse radiation, since according to Table 6, AMF_{Dif} takes values greater than 1, that become even greater the higher the AOD (more aerosol present). Unlike before, this enhancement is bigger than the uncertainty, which leads us to conclude that aerosols' scattering can cause the diffuse radiation to increase.

- In turn, direct irradiance acts oppositely, getting lower when AOD increases. Logically, the higher the quantity of aerosols, the greater the chance of incident radiation being scattered by them, and therefore being classified as diffuse radiation instead of direct. This effect is a bit more relevant than that enhancing of diffuse, as we can see global radiation as a whole decreases slightly with AOD.

- Diffuse radiation also presents a notable dependence on wavelength specially relevant when there is a high presence of cloud or aerosols: at λ closer to the visible range, CMF/AMF grows significantly.

- Moreover, for both cloud and aerosol effect, CMF/AMF is found to decrease with SZA. This can be explained if we note that the lower the sun is (high SZA), the bigger the optical path length and the optical mass that radiation goes through, making back-scattering processes (that prevent incident radiation from reaching the surface) more likely to happen.

- The general increase of SD for SZA = 15° responds to the fact that this range of angles has the least data and therefore, a more sensitive average AMF.

9. Conclusions

Finally, after completing the study and discussing its results, the following conclusions were reached:

1. According to the statistical parameters obtained, the simulations are quite close to the experimental measurements, and therefore valid as a clear sky model for our calculations. In the case of global radiation, they can be considered highly correlated, since it –being their sum– compensates in a certain way for the deviations of its components, losing a part of that correlation when it unfolds in them.

2. A decreasing trend of the CMF with wavelength has been found. This dependence is more noticeable in the case of direct radiation and for skies more covered by clouds than for global radiation or those skies with less clouds. A possible explanation for this decrease in CMF in cloudy skies for global radiation would be understood from Rayleigh scattering, which scatters much more radiation when the wavelength is shorter (see (1)), redirecting part of the radiation scattered by clouds to the surface.

   Although, it has been noticed that this does not occur when treating with diffuse radiation and a significant cloud cover or aerosol presence, where it seems to have the opposite tendency. This happens because the role of the diffuse component is dominant at short wavelenghts and high SZA, where ozone absorption is relevant (Mateos et. al, 2014) [26]

3. It has been observed that the CMF clearly decreases as the skies become more covered by clouds, both for global and direct radiation, showing that clouds have an attenuating effect on UV radiation. Direct radiation is found to be noticeably more sensitive to the presence of clouds, since a greater number of clouds implies a greater number of drops (or ice crystals) suspended in the atmosphere that can absorb or scatter

it, preventing direct radiation from reaching the ground without interacting with one of these water droplets (or ice crystals). Quantifying this mitigating effect, the extinction of more than half of the global radiation for overcast skies (8 oktas) has been observed, most of which was direct radiation, reduced up to almost 95%, for only around 36% of diffuse.

4. AMF has also been found to decrease for global and direct radiation as the aerosol present becomes more abundant, accounting for a mitigating effect aerosols have on UV radiation. When AOD takes high values, around 16% of global radiation goes extinct, while for direct radiation that reduction is much greater, of up to almost 60%, since the bigger quantity of aerosol particles makes it more possible that the radiation undergoes a extinction process. On the other hand, AMF_{Dif} takes higher values the greater the AOD is (up to a 45% increase), implying an enhancing effect of aerosols on diffuse radiation.

5. Furthermore, it was observed that CMF and AMF decrease with greater SZAs, as that implies a longer optical path and optical mass, which leads to the radiation having a bigger opportunity of interacting with a cloud or aerosol particle and go extinct.

Future lines of work can include the study of other aerosol properties like Ångström's exponent, α, to look for a dependence of radiation on the size of the aerosols present, as well as the study of the effect of another atmospherical components of great relevance, such as gases (specially ozone).

References

[1] A. C. de la Casinière and V. E. Cachorro. *La radiación solar en el sistema tierra-atmósfera.* Ciencias (Universidad de Valladolid), 2008.

[2] B. L. Diffey. Sources and measurement of ultraviolet radiation. *Methods*, 28(1):4–13, September 2002.

[3] J. Reichrath and S. Reichrath. Hope and challenge: the importance of ultraviolet (UV) radiation for cutaneous vitamin D synthesis and skin cancer. *Scandinavian Journal of Clinical and Laboratory Investigation Supplement*, 243:112–119, April 2012.

[4] Organización Mundial de la Salud. *Índice UV Solar Mundial. Guía práctica.* Accedido en 21-04-21 a http://www.who.int/entity/uv/publications/en/uvispa.pdf, 2003.

[5] B. L. Diffey. Solar ultraviolet radiation effects on biological system. *Physics in Medicine and Biology*, 36:299–328, 1991.

[6] J. Krutmann. III. Immunology of UV-irradiated skin. *European Journal of Cancer*, 30(4):554–555, 1994.

[7] R. Román. *Reconstrucción y análisis de la radiación ultravioleta eritemática en la Península Ibérica desde 1950.* PhD thesis, UVa, 2014.

[8] D. Mateos. *Solar Irradiance and Actinic Flux in the UV Range: Advances in the Characterization of the Cloudy Scenario.* PhD thesis, UVa, 2012.

[9] F. Velázquez de Castro. *El ozono: ¿cuándo protege y cuándo destruye?* McGraw-Hill Interamericana de España, 2001.

[10] F. Q. Zhao and H. Hiroyasu. The applications of laser rayleigh scattering to combustion diagnostics. *Progress in Energy and Combustion Science*, 19(6):447–485, 1993.

[11] F. Robben. *Comparison of density and temperature measurement using Raman scattering and Rayleigh scattering*, pages 179–195. Lawrence Berkeley National Laboratory, 1975.

[12] M. Kerker. *The Scattering of Light and Other Electromagnetic Radiation.* Academic Press, 1969.

[13] E. J. McCartney. *Optics of the Atmosphere (Scattering by Molecules and Particles).* John Wiley & Sons, Nueva York, 1976.

[14] J. Calbò, D. Pagès, and J.-A. González. Empirical Studies of Cloud Effects on UV Radiation: A review. *Reviews of Geophysics*, 43(2):1–28, 2005.

[15] C. Fröhlich and J. London. *Revised instruction manual on radiation instruments and measurements*. WCRP publications series nº 7. WMO/TD nº 149, October 1986.

[16] J. G. Estupiñán, S. Raman, G. H. Crescenti, J. J. Streicher, and W. F. Barnard. Effects of clouds and haze on UV-B radiation. *Journal of Geophysical Research*, 101:16807–16816, July 1996.

[17] J. S. Schafer, V. K. Saxena, B. N. Wenny, W. Barnard, and J. J. DeLuisi. Observed influences of clouds on ultraviolet-B radiation. *Geophysical Research Letters*, 23:2625–2628, September 1996.

[18] C. Toledano. *Climatología de los aerosoles mediante la caracterización de propiedades ópticas y masas de aire en la estación "el arenosillo" de la red AERONET*. PhD thesis, UVa, 2005.

[19] R. Román, D. Mateos, A. de Miguel, J. Bilbao, A. Pérez-Burgos, R. Rodrigo, and V.E. Cachorro. Atmospheric effects on the ultraviolet erythemal and total shortwave solar radiation in Valladolid, Spain. *Óptica Pura y Aplicada*, 45:17–21, January 2012.

[20] M. J. Marín, A. R. Esteve, F. Tena, M. P. Utrillas, and J. A. Martínez-Lozano. UVI dependence on ozone amount and turbidity in Valencia. *Óptica Pura y Aplicada*, 40(1):25–30, 2007.

[21] M. Antón, R. Román, A. Valenzuela, F. J. Olmo, and L. Alados-Arboledas. Direct-sun total ozone data from a spectroradiometer: methodology and comparison with satellite observations. *Atmospheric Measurement Techniques*, 6:637–647, 2013.

[22] R. Román, M. Antón, A. Valenzuela, J. E. Gil, H. Lyamani, A. De Miguel, F. J. Olmo, J. Bilbao, and L. Alados-Arboledas. Evaluation of the desert dust effects on global, direct and diffuse spectral ultraviolet irradiance. *Tellus Series B: Chemical and Physical Meteorology*, 65(1):19578, 2013.

[23] A. Cazorla, F. J. Olmo, and L. Alados-Arboledas. Development of a sky imager for cloud cover assessment. *Journal of the Optical Society of America A*, 25(1):29–39, January 2008.

[24] AERONET (*Aerosol Robotic Network*): http://aeronet.gsfc.nasa.gov.

[25] *Guía de usuario de LibRadtran* disponible en http://www.libradtran.org.

[26] D. Mateos, A. di Sarra, J. Bilbao, D. Meloni, G. Pace, A. de Miguel, and G. Casasanta. Spectral attenuation of global and diffuse UV irradiance and actinic flux by clouds. *Quarterly Journal of the Royal Meteorological Society*, 141:109–113, January 2015.